Voltage Tuning of Gain Spectra in Quantum Cascade Lasers

Yu Yao*[a], Kale J. Franz[a], Zhijun Liu[a,b], Anthony J. Hoffman[a], and Claire F. Gmachl[a]

[a] Dept. of Electrical Engineering, Princeton Univ., Princeton, NJ, USA 08544;
[b] Current address: Division of Engineering, Brown Univ., Providence, RI, USA 02912

ABSTRACT

The voltage tuning of gain spectra in three types of Quantum Cascade laser designs is investigated. The gain spectra of the luminescence device are tunable over the whole voltage operation range for all designs. The lasers are as tunable as the electroluminescence below threshold, while a reduced tunability is observed in all lasers above threshold. This is attributed to the decrease of resistance across the laser active region as the photon density increases. A resumed tunability high above threshold occurs in all lasers based on the anti-crossed designs. Lasers based on the anti-crossed diagonal transition are tunable above threshold, with a tuning range of about 40 cm^{-1} (~4% of the laser emission wavenumber) at room temperature, i.e. a tuning rate of 800 cm^{-1} per volt per period of active region and injector.
Keywords: Semiconductor lasers, quantum cascade lasers, tunable lasers, Stark effect

1. INTRODUCTION

Quantum Cascade (QC) lasers are ideal candidates for mid-infrared spectroscopy because their emission wavelength can be designed in the mid-to-far-infrared range from 2.7 μm to 24 μm [1, 2] and THz range. A broad wavelength tuning range is required for lasers in many applications. In the detection of multiple trace-gases or chemical species with interfering absorption features, for example, it is necessary to tune the laser wavelength over a wide range. Broad tunability requires a gain medium that can provide gain over a wide wavelength range. Heterogeneous active regions [3] or bound-to-continuum designs [4] can be used to achieve a broader gain spectrum. However, both come at the cost of the peak gain. An alternative method would be a widely tunable gain spectrum.

Voltage tuning of QC lasers based on a strong linear Stark effect in quantum wells is expected to function at a much higher tuning speed than the temperature tuning. The tuning coefficient is proportional to the spatial distance between the centroids of the electron probability distributions of the upper and lower laser states [5]. Theoretically, one can achieve very large tuning coefficients by increasing the spatial distance between the two states. Faist et al. [6] demonstrated a broad tuning range of the intersubband electroluminescence (EL) (over 220 cm^{-1}) in a structure based on photon-assisted tunneling. However, above threshold, the lasers are not tunable.

We have recently investigated and reported the voltage tunability of three types of QC laser designs, i.e. the anti-crossed vertical design, the anti-crossed diagonal design and the 'super' diagonal design [7]. Here we review this work and add to it the voltage tuning of gain spectra above threshold in the anti-crossed diagonal design and the simulation results of a rate equation model to explain the observed tuning behavior for lasers above threshold. The paper is arranged as follows. Part II gives a detailed explanation of the experiments. In part III, the tunability of both luminescence and laser devices of all three designs is studied. The luminescence devices are all tunable. All lasers have reduced tunability above threshold; however, lasers based on an anti-crossed diagonal transition active region can be tuned over 30 cm^{-1} and 40 cm^{-1} (3% and 4% of the laser emission wavenumber) above threshold at 80K and 295K, respectively, with a tuning coefficient of 750 cm^{-1} and 800 cm^{-1} per volt per period of active region and injector because of a resumed tunability. In Part IV, the anti-crossed diagonal design is further investigated by cleaving the laser stripes in the direction perpendicular to its facets and measuring the lateral emitted EL above threshold at room temperature. The peaks of gain spectra inside the laser cavity below and above threshold are obtained and compared with the wavenumbers of corresponding laser emission spectra. Part V presents a simplified rate equation model to explain the reduced tunability of laser spectra above threshold. Part VI is the conclusion.

Novel In-Plane Semiconductor Lasers VIII, edited by Alexey A. Belyanin, Peter M. Smowton,
Proc. of SPIE Vol. 7230, 723012 · © 2009 SPIE · CCC code: 0277-786X/09/$18 · doi: 10.1117/12.808295

2. EXPERIMENT

The samples studied in this paper are based on three different types of QC laser designs. Fig. 1 (a) shows an anti-crossed vertical transition design (sample AVQ) [8]. Fig. 1(b) is an anti-crossed diagonal transition design (sample ADQ) [9]. Both of them are widely used at present in achieving high performance QC lasers. Fig. 1 (c) shows a diagonal transition design based on photon-assisted tunneling ("super" diagonal design, sample SDQ) [10].

All three samples were processed into 200-μm-diameter circular mesas. The mesas were etched past the active core with slanted side-walls to ensure that the electroluminescence would not be impacted by any cavity effect; for each sample, ridge lasers were also processed for different threshold current densities by changing the width and the length of the laser cavity. All lasers are based on a Fabry-Perot (FP) cavity with as-cleaved facets. The EL from the mesas was

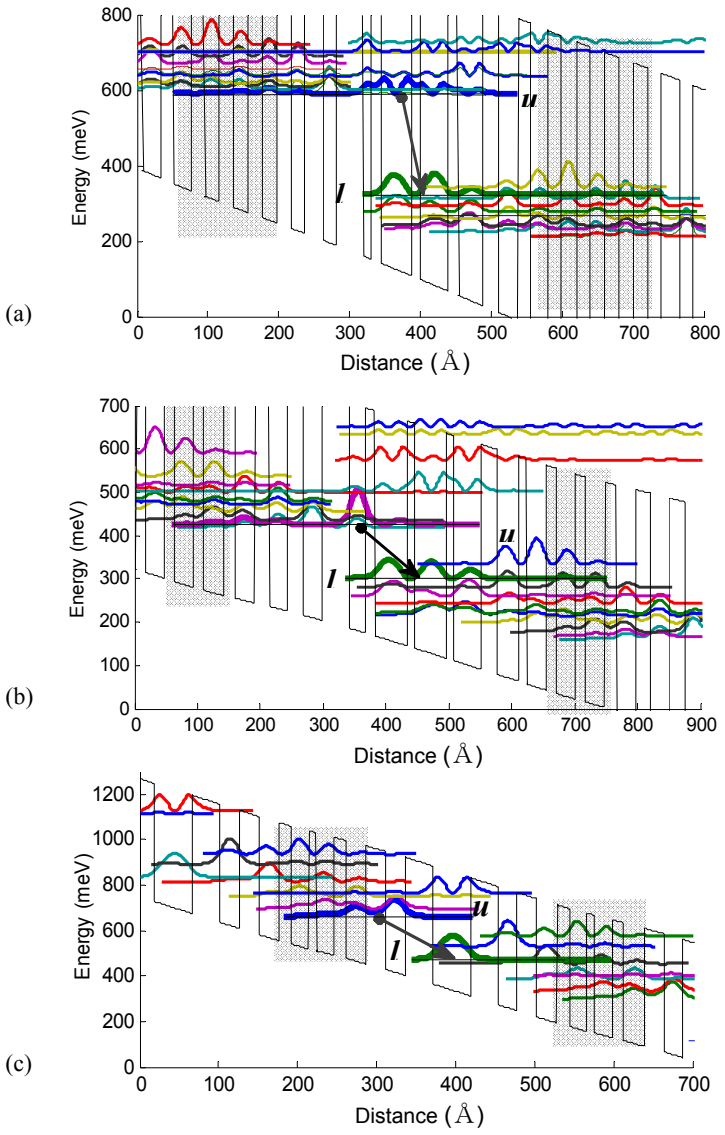

Fig. 1. Conduction band diagram of a portion of the active regions and injectors and the moduli squared of the relevant wave functions of (a) sample AVQ under an average electric field of 75kV/cm; (b) sample ADQ under an average electric field of 43kV/cm; (c) sample SDQ under an average electric field of 100 kV/cm. The bold curves represent the upper and lower laser states. The arrows indicate the respective laser transitions. The shaded regions indicate the doped layers. All structures are calculated with a self-consistent Poisson-Schrödinger solver.

measured in pulsed mode using a Fourier-transform infrared spectrometer (FTIR) with a cooled HgCdTe (MCT) detector. The EL of lasers below threshold and laser spectra above threshold were also measured at the same condition.

The peak wavenumber of EL can be determined by fitting the raw data with (if necessary, multiple) Gaussian or Lorentzian peaks and selecting the peak value of the fitted curve, as shown in Fig 2 (a). The asymmetry of the electroluminescence is because of multiple optical transitions that co-occur in the quantum well structures. Fig. 2 (b) shows the spectra of a laser based on the anti-crossed diagonal design (sample ADQ) at different injection current densities. The spectrum broadens as the current density increases, splitting into two or three humps when the driving current exceeds a certain value. This phenomenon was found in most of the lasers measured in our study. The broadening of the laser spectra has several reasons: spatial hole burning, Rabi splitting [11] and wavelength dependent loss (introduced by material defect or waveguide non-uniformity, e.g.). To determine the tuning trend of the laser spectra, we measured the wavenumbers on both sides at half height of the peak intensity and extracted the mid-point value for the laser wavenumber. This method gives consistent results for lasers based on the same design.

Lasers based on the diagonal transition design are cleaved in the direction perpendicular to its facet to detect intersubband spontaneous emission from the laser above threshold [12]. A scanning electron micrograph (SEM) of such a cleaved device is shown in Fig. 3 (a). Light from the long cleaved side is measured in pulsed mode using a FTIR with a

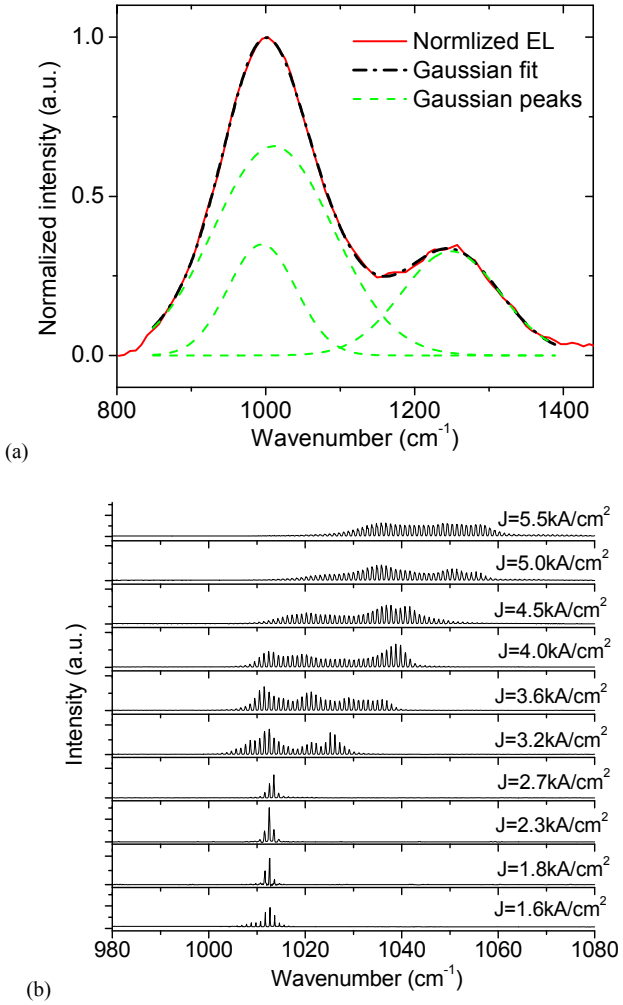

Fig. 2. (a) Electroluminescence from a mesa based on the anti-crossed diagonal design (sample ADQ); (b) spectra of a laser (sample ADQ) at different injection current densities. Both graphs are taken at T=80K in pulsed mode (80kHz, 100ns pulse width).

cooled MCT detector. Laser emission is also detected from the lateral cleaved side because of scattering from defects inside the cavity (scattered light from outside the cavity can be blocked by putting a pin hole in front of the laser lateral facet). Fig. 3 (b) shows the intersubband EL and scattered laser emission for a laser at an injection current 20% above threshold. The peak wavenumber of the intersubband EL is obtained by cutting the strong laser emission peak and fitting the EL data with Gaussian or Lorentzian peaks, as also shown in Fig. 3 (b). One can see that the wavenumber of the laser emission spectra is close to the EL peak.

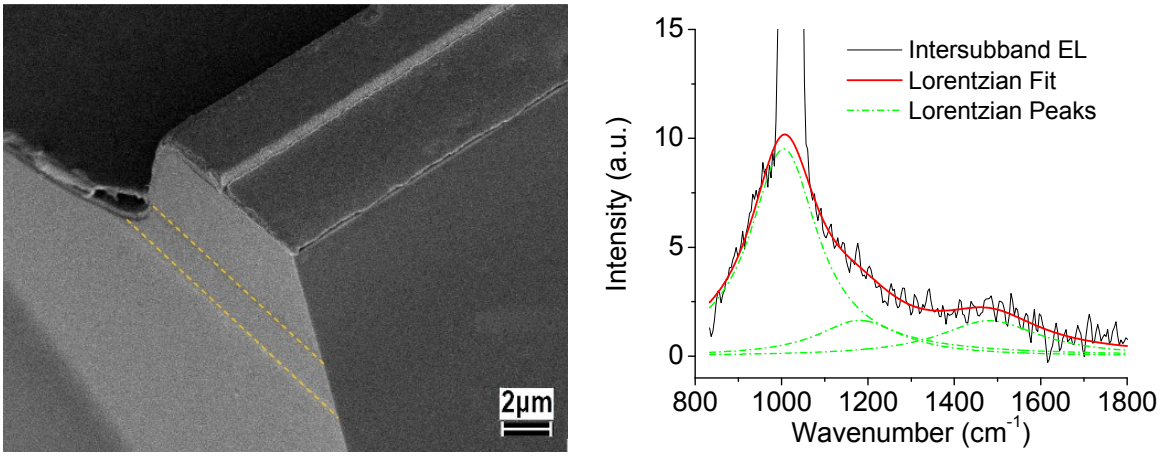

(a) (b)

Fig. 3. (a) SEM of the cleaved facets of a laser. The region between the dashed lines indicates the active waveguide core. (b) Intersubband EL detected through the lateral cleaved facet (the right cleaved facet in Fig. 3. (a)) from a laser 20% above threshold at room temperature (~295K) in pulsed mode (80kHz, 50ns pulse width) and the fitted curve.

3. TUNABILITY OF ELECTROLUMINESCENCE AND LASER SPECTRA

As mentioned previously, the voltage tuning of the intersubband EL is a consequence of the linear Stark effect in the quantum wells. The EL tuning coefficient is proportional to the spatial distance between the two transition states [5, 6].

$$\frac{dE_{ph}}{dF} = q(z_l - z_u) \tag{1}$$

Where E_{ph} is the transition energy, F is the electrical field in the active region, q is the electron charge, and z_l, z_u are the coordinates of the centroids of the electron probability distributions at the lower and upper laser states, respectively. The electron probability distributions change with applied electric fields. Therefore, we employ a self-consistent Poisson-Schrödinger solver to calculate the band structure at different electric fields, considering the impact of electron distribution on the local electric field according to Gauss law. The results are shown in Figs. 3 (a), (b) and (c) for the anti-crossed vertical design, anti-crossed diagonal design and 'super' diagonal design, respectively.

The measured EL peak wavenumbers of mesas are also shown in Figs. 3 as functions of the voltage drop over each period of active region and injector for all three structures. The corresponding average electric field over the injectors and active regions is also given on the top axes. The tuning coefficient can be calculated as:

$$\frac{dE_{ph}}{dF_{ave}} = \frac{dE_{ph}}{dV_p} L_p \tag{2}$$

Where V_p is the voltage over one period and L_p is the length of one period and F_{ave} is the average electric field over the active region and injector in the core of the QC laser structure. Both calculated and measured EL tuning coefficients for all three samples are shown in Table 1. The measured results show that the "super" diagonal design has the largest tuning

coefficient, followed by the anti-crossed diagonal design, while the anti-crossed vertical design has the smallest tuning coefficient. However, the calculated results show the largest tuning coefficient for the anti-crossed diagonal design and the smallest tuning coefficient for the "super" diagonal design. This overestimation of tuning coefficients for the anti-crossed designs has also been found by A. Müller et al. [13]

Table 1. Tuning coefficients of electroluminescence.

Sample	Measured (cm-1 per kV/cm)	Calculated (cm-1 per kV/cm)
AVQ	1.04 (Vp>0.332V)	8.98
(Anti-crossed vertical)	3.06 (Vp<0.332V)	
ADQ	3.76	13.2
(Anti-crossed diagonal)		
SDQ	5.21 (Vp>0.34V)	8.12
("Super" diagonal)	13.17 (Vp<0.34V)	

Vp: Voltage per period

For the anti-crossed vertical and diagonal designs, the upper and lower laser states are widely distributed across the quantum wells when they come into anti-crossing with the injector states, which results in a very large spatial distance between the upper and lower laser states. However, because of various scattering mechanisms which are not included in the calculation, the electron probability distributions are more localized than calculated. If we take this into consideration, a smaller spatial distance is expected. Therefore, the real tuning coefficients are smaller than the calculated results.

We also notice that for some designs, the tuning coefficients change with the applied voltage. For example, the anti-crossed vertical design has a much larger tuning coefficient for an applied voltage per period below 0.33V than for the voltage above that. The likely reason is the electron screening as mentioned in ref. [6]. When the applied voltage is low, more and more extrinsic electrons from the doped region relax to the injection barrier as the voltage is increased. As a result, the positive charge in the doped region and the extrinsic electrons generate a stronger built-in electric field, which is in the opposite direction to the applied field. This leads to a smaller increase of electric field in the injectors but a larger increase of electrical field in the active region. In the following, this voltage range will be referred as the screening region. When the voltage is large enough, most of the electrons are accumulated in front of the injection barrier. A further increase of voltage will lead to little change in the electron distribution. Therefore, only above the screening region, the change of the electric field and the voltage over one period are linearly related,

$$dF = \frac{dV_p}{L_p} = dF_{ave} \tag{3}$$

which means that the increase of voltage will result in uniform increase of the electric field over the active region and injector, even though the electric field is not uniform.

The measured results show an EL tuning range of about 40cm^{-1} for the anti-crossed vertical design (AVQ), 90 cm^{-1} for the anti-crossed diagonal design (ADQ), and 190 cm^{-1} for the "super" diagonal design (SDQ), i.e. 2%, 9%, and 12.5% of their EL peak wavenumbers, respectively. The diagonal designs have much larger tuning ranges as well as tuning coefficients than the vertical design, certainly because of a larger spatial distance. This spatial distance can be made larger by engineering the band structure or reducing the scattering in quantum wells.

The peak wavenumbers of the laser spectra are also shown in Figs. 3. All the lasers are tunable below threshold. However, their tunability is reduced above threshold. For the anti-crossed vertical design, the wavenumbers decrease first and then start to increase again after a certain voltage (0.35V for sample AVQ). For lasers based on the anti-crossed diagonal design, the wavenumbers are almost constant just above threshold, but the tunability approaches that of the EL after the voltage over one period is higher than 0.28V. Lasers based on the "super" diagonal design have almost no tuning above threshold.

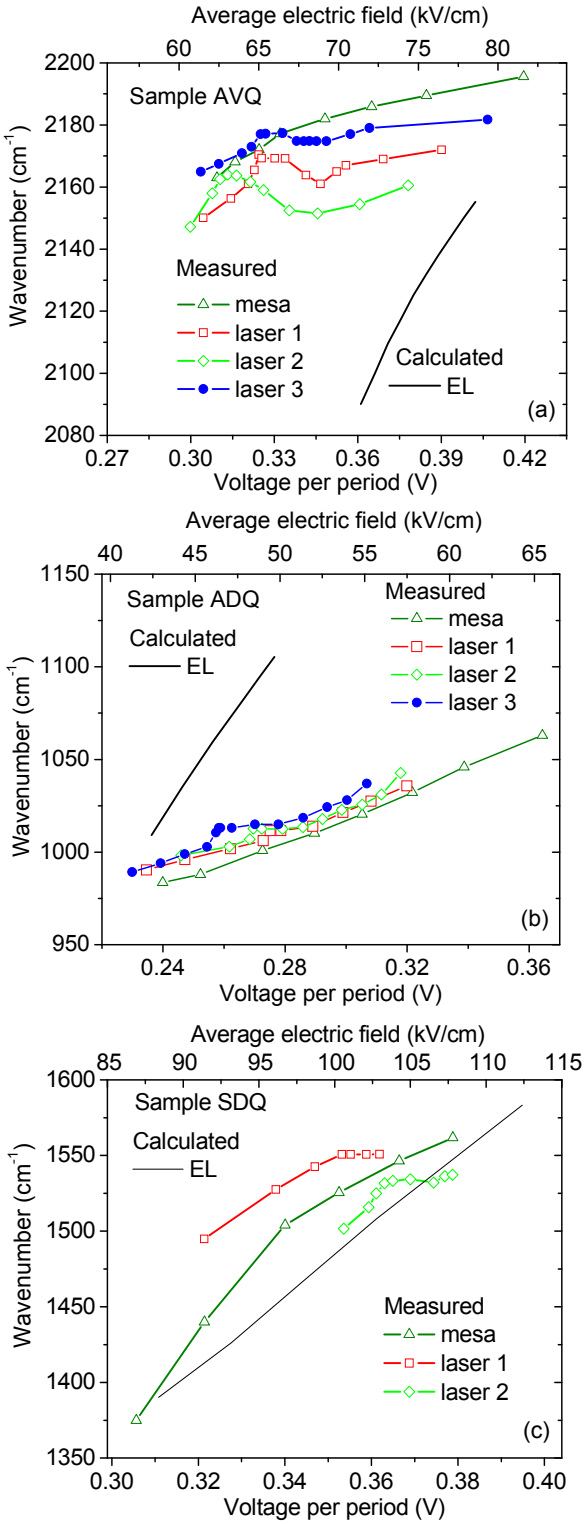

Fig. 4. (a) Anti-crossed vertical design (sample AVQ). (b) Anti-crossed diagonal design (sample ADQ). (c) "Super" diagonal design (sample SDQ). Calculated EL peak (Solid lines) and measured EL peak and laser emission wavenumbers (Symbols) as functions of the voltage drop per period of active region and injector (bottom axis) and average electric field (top axis). Experimental data are measured at 80K in pulsed mode (80kHz, 100ns pulse width).

4. GAIN SPECTRA OF LASERS

The laser emission spectra are not only determined by the gain spectra but also dependent on some other factors such as wavelength dependent loss, spatial hole burning, etc. Therefore, the laser emission wavenumbers are not necessarily the same as the gain spectra peak wavenumbers. To obtain the gain spectra of a laser above threshold, we employ a method proposed by R. Colombelli et al [12], a direct way to measure the intersubband EL from lasers both below and above threshold. By cleaving the laser ridge along the direction perpendicular to its facets, the EL can be measured from the lateral side because it is isotropic in all directions while laser emission is along the cavity longitudinal axis. In this way, the gain spectra can be obtained directly from the measured EL. Fig. 5 (a) shows the EL spectra from a laser at different injection current densities. Ideally, the lateral emitted photons are all originated from spontaneous emission; however, because of scattering from defects inside the cavity, the scattered laser emission light is also collected. Therefore, all the data above threshold have a strong peak at the laser emission wavenumbers, which shows the laser emission spectra as well as the EL spectra. The EL peaks are obtained from the fitted curve of the EL data, as show in Fig. 3 (b). Both the EL peaks and laser emission wavenumbers are plotted as a function of voltage per period of active region and injector in Fig. 5 (b). Here we show the results for two lateral cleaved lasers (laser 1 and laser 2). One can see the laser emission wavenumbers are close to the EL peaks; more importantly, the tuning of laser spectra follows that of the EL peaks. We also measured the EL and emission spectra from a laser (laser 3) without cleaving along the ridge. Its tuning behavior is similar to the lateral cleaved lasers. Both the laser spectra and the lateral emitted EL have reduced tunability just above threshold, yet a resumed tunability higher above threshold.

All these experimental results show that the gain spectra peaks and emission wavenumbers of lasers above threshold match with each other quite well, indicating the way we determine the laser emission wavenumbers, as mentioned in part II, gives good estimation of the gain spectra peaks. Moreover, all lasers show similar tuning behaviors as those at 80K; the tuning range of the gain spectra for the anti-crossed diagonal design is not reduced at room temperature compared with that at 80K. The largest tuning range achieved at 295K is 40 cm^{-1}, i.e. a tuning rate of 800 cm^{-1} per volt per period of active region and injector.

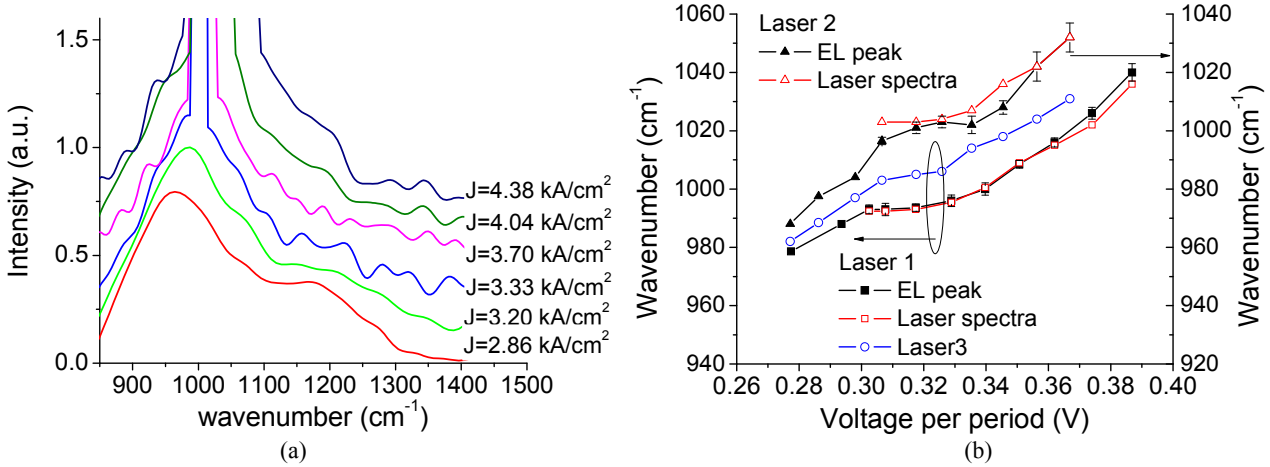

Fig. 5. (a) Sub- and above-threshold spectra of a laser based on anti-crossed diagonal design. (b) EL peak wavenumber and laser emission wavenumber from two lateral cleaved laser samples (laser 1 and laser 2) and one laser without cleaving along its ridge (laser 3). The error bars show the standard deviations of the mean peak. All experimental data are measured at ~295 K in pulsed mode (80kHz, 50ns pulse width).

5. REDUCED TUNABILITY

Since the lasers and mesas are made from the same wafers, they have identical active cores (active regions and injectors) and waveguide structures. The most significant difference between lasers and mesas is that the stimulated emission strongly influences the lasers' optical and electrical behavior above threshold. For all three designs, the voltage over the laser active core becomes smaller than that of the mesas above threshold and all the lasers experience a drop in differential resistance at threshold, while the differential resistance of mesas is continuous [7]. An understanding of these

observations can be achieved by analyzing the effect of the stimulated emission on the active region. Starting from the rate equation of the electron population in the upper laser state,

$$\frac{dN_u}{dt} = R_u - \frac{N_u}{\tau_u} - \sigma \Delta N \, \varphi \tag{4}$$

Where N_u, ΔN are the population on the upper laser state and the population inversion between the upper and the lower laser states, respectively; R_u is the electron pumping rate into the upper laser state; τ_u is the phonon scattering lifetime of the upper laser state; σ is the gain cross-section and φ is the photon flux in the cavity.

Below threshold, the stimulated emission (the third term on the right in Eq. (4)) can be omitted. However, above threshold, a large portion of the electrons at the upper laser state will transit to the lower laser state via stimulated emission, which results in faster depopulation of the upper laser state. If we include the stimulated emission term into the second term in Eq. (4), we can define an effective lifetime for the upper laser state, τ_u^{eff}:

$$\frac{1}{\tau_u^{eff}} = \frac{1}{\tau_u} + \frac{\Delta N}{N_u}\sigma\varphi \tag{5}$$

$$\frac{dN_u}{dt} = R_u - \frac{N_u}{\tau_u^{eff}} \tag{6}$$

Above threshold, the light intensity in the cavity is increased as the injection current increases. Therefore, the effective lifetime of the upper laser state becomes smaller, according to Eq. (5). This has been verified in the femtosecond time-resolved pump-probe measurement recently by H. Choi et al [14]. Here we apply a rate equation model to simulate anti-crossed diagonal design, with the parameters calculated with the self-consistent Poisson-Schrödinger solver. The light-current-voltage characteristics as well as the lifetime of the upper laser state as a function of current density are shown in Fig. 6. The simulation results that the upper laser state lifetime reduces from 2.8 ps below threshold to less than 1.7 ps as the injection current increases to 1.7 times above threshold. The decrease of the effective lifetime of the upper laser state results in a reduced resistance in the active region, i.e. as the light intensity inside the cavity becomes stronger and stronger, more and more electrons transit across the active region via stimulated emission. Therefore, when the current density goes up, most of the voltage increase is across the injectors; the electrical field in the active region does not grow as fast.

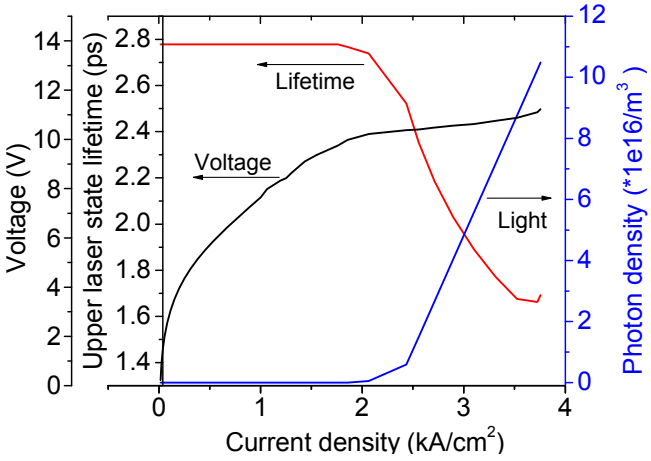

Fig. 6. Results of numerical simulation of laser above threshold based on rate equations including stimulated emission and parameters obtained from the self-consistent Poisson-Schrödinger solver.

6. CONCLUSION

The voltage tunability of intersubband EL is mainly determined by the spatial difference of the upper and lower laser states. The tuning ranges for the 'super' diagonal, anti-crossed diagonal and anti-crossed vertical design are 190 cm^{-1}, 90cm^{-1} and 40 cm^{-1}, i.e. 12.5%, 9%, and 2% of their EL peak wavenumbers, respectively. The comparison of measured and calculated tuning coefficients shows a large overestimation for designs based on resonant tunneling. The explanation is that the scattering in quantum wells (because of roughness, impurities, etc.) results in more localized electron probability distributions and therefore, leads to a smaller tuning coefficient than calculated.

Lasers above threshold show a different tunability from the EL. The intersubband EL measured from lateral cleaved laser facets confirmed a reduced tuning rate of the gain spectra at threshold. The explanation lies in the stimulated emission, which leads to the drop of resistance at threshold in lasers. Moreover, the dramatic increase of light intensity above threshold makes the resistance of active region decrease as the current density increases. Thus the electric field over the active region does not increase as much as that over the injectors.

A resumed tunability has been observed in anti-crossed designs. A comparison of the results of the anti-crossed designs with that of the "super" diagonal design suggests that this is due to the anti-crossing of the ground state in the injector with the upper laser state. Lasers based on the anti-crossed diagonal design have a tuning range of about 40 cm^{-1} (4% of the laser emission wavenumber) above threshold and a tuning coefficient of 800 cm^{-1} per volt per period of active region and injector at room temperature. Further research is needed on understanding the resumed tunability and improving the tuning range of anti-crossed diagonal designs.

ACKNOWLEDGMENT

The authors acknowledge the assistance of X.Wang and J. Fan at AdTech Optics, City of Industry, CA, F. J. Towner at Maxion Technologies Inc., Hyattsville, MD, and D. L. Sivco at Alcatel-Lucent, Murray Hill, NJ for wafer growth. This work was supported in part by MIRTHE (NSF-ERC).

REFERENCES

[1] C. Gmachl, F. Capasso, D. L. Sivco, and A. Y. Cho, "Recent progress in quantum cascade lasers and applications," Rep. Prog. Phys., vol. 64, pp. 1533–1601 (2001).

[2] R. Teissier, J. Devenson, O. Cathabard, A. N. Baranov, "Short wavelength quantum cascade lasers emitting around 3μm," presented at the Conference on lasers and electro-optics, San Jose, CA, May 4-9, 2008, paper CTuF4.

[3] C. Gmachl, D. L. Sivco, R. Colombelli, F. Capasso, and A. Y. Cho, "Ultra-broadband semiconductor laser," Nature, vol. 415, pp. 883 – 887 (2002).

[4] J. Faist, M. Beck, T. Aellen, E. Gini, "Broadband tuning of external cavity bound-to-continuum quantum-cascade lasers," Appl. Phys. Lett. Vol. 84, pp. 1659 (2004).

[5] P. F. Yuh and K. L. Wang, "Large stark effects for transitions from local states global states in quantum well structures," IEEE J. Quantum Electron, vol. 25, no. 7, pp. 1671-1676 (1989).

[6] J. Faist, F. Capasso, C. Sirtori, D. L. Sivco, A. L. Hutchinson, and A. Y. Cho, "Laser action by tuning the oscillator strength," Nature, vol. 387, pp. 777-782 (1997).

[7] Y. Yao, Z. Liu, A. J. Hoffman, K. J. Franz, C. F. Gmachl, "Voltage tunability of quantum cascade lasers," IEEE J. Quantum Electron, accepted (2008).

[8] A. Evans, J. S. Yu, S. Slivken, and M. Razeghi, "Continuous-wave operation of λ~4.8 μm quantum-cascade lasers at room temperature,"Appl. Phys. Lett. vol. 85, pp. 2166 (2004).

[9] Z. Liu, C. F. Gmachl, L. Cheng, F. Choa, F. J. Towner, X. Wang, and J. Fan, "Temperature-dependent gain and loss in room-temperature continuous-wave quantum cascade lasers between 8.2-10.3μm," IEEE J. Quantum Electron, vol. 44, no. 5, pp. 485-492 (2008).

[10] C. Gmachl, A. Tredicucci, D. L. Sivco, A. L. Hutchinson, F. Capasso, A. Y. Cho, "Bidirectional semiconductor laser," Science, vol 286, pp. 749-752 (1999).

[11] C. Y. Wang, L. Dieh, A. Gordon, C. Jirauschek, F. X. Kärtner, A. Belyanin, D. Bour, S. Corzine, G. Höfler, M. Troccoli, J. Faist, and F. Capasso, "Coherent instabilities in a semiconductor laser with fast gain recovery," Physical review A, vol 75, pp. 031802(R) (2007).
[12] R. Colombelli, F. Capasso, C. F. Gmachl, A. Tredicucci, A. M. Sergent, A. L. Hutchinson, D. L. Sivco, and A. Y. Cho, "Intersubband electroluminescence from long-side-cleaved quantum-cascade lasers above threshold: Investigation of phonon bottleneck effects," Appl. Phys. Lett. Vol. 85, pp. 3893 (2000).
[13] A. Müller, M. Beck, J. Faist, U. Oesterle and M. Ilegems, "Electrically tunable, room-temperature quantum-cascade lasers," Appl. Phys. Lett., vol. 75, no. 11, pp. 1509 (1999).
[14] H. Choi, L. Diehl, Z. Wu, M. Giovannini, J. Faist, F. Capasso, and T. B. Norris, "Gain recovery dynamics and photon-driven transport in quantum cascade lasers," Phys. Review Lett. vol. 100, no. 16, pp. 167401 (2008).